Hybrid-Electric Aero-Propulsion Controls Testbed Results

Jonah J. Sachs-Wetstone[1], Santino J. Bianco[2], Jonathan L. Kratz[3],
NASA Glenn Research Center, Cleveland, OH, 44135, USA

Marcus A. Horning[4],
HX5, LLC, Brook Park, OH, 44142, USA

Aria E. Amthor[5], Joseph W. Connolly[6], Joseph R. Saus[7]
NASA Glenn Research Center, Cleveland, OH, 44135, USA

NASA is supporting the development of Electrified Aircraft Propulsion (EAP) technology due to its potential to reduce aircraft fuel burn, emissions, and noise as well as improving safety and performance. One focus of this research is the electrification of conventional turbomachinery propulsion systems, which offers ways to improve the performance and operability of turbine-engine powered aircraft through the addition of electro-mechanical systems. These hybrid-electric turbine engines provide additional actuation and energy management control opportunities for improving stability and transient response behavior. This paper summarizes the results of a Hardware-in-the-Loop (HIL) test performed at the NASA Electric Aircraft Testbed (NEAT) during the summer of 2022. The test demonstrates the feasibility and performance of an advanced energy management control strategy by integrating a simulated turbofan engine with scaled electro-mechanical hardware. A full-scale real-time reference model of a geared turbofan was run alongside a scaled electro-mechanical system representing the electrified turbofan components operating at a megawatt-scale power level. The model was interfaced with the hardware through a novel closed-loop control and scaling algorithm that emulated the dynamic speed and torque response of the turbofan shafts. The control strategy was implemented on the electrical machines connected to the emulated turbomachinery shafts. The results from the testbed are compared against simulations that predict the testbed and geared turbofan model operation. The energy management control strategy successfully changed the operating point of the engine model and improved its stability during throttle transients. These results also demonstrate the success of the novel closed loop control and scaling approach for emulating turbomachinery and elevate the Technology Readiness Level (TRL) of the energy management control strategy.

I. Nomenclature

F_{net} = net thrust, lbf

[1] Aerospace Engineer, Intelligent Control and Autonomy Branch, AIAA Member.
[2] Control Systems Engineer, Intelligent Control and Autonomy Branch, AIAA Member.
[3] Control Systems Engineer, Intelligent Control and Autonomy Branch, AIAA Senior Member.
[4] Aerospace Engineer, Intelligent Control and Autonomy Branch. Non-AIAA Member
[5] Control Systems Engineer, Intelligent Control and Autonomy Branch, AIAA Member.
[6] Aerospace Engineer, Intelligent Control and Autonomy Branch, AIAA Associate Fellow.
[7] Aerospace Engineer, Intelligent Control and Autonomy Branch, AIAA Senior Member.

N_{1c} = corrected fan speed, rpm
N_2 = LPS speed, rpm
N_3 = HPS speed, rpm
P_3 = static pressure at station 3 (high pressure compressor discharge), psi
SM = stall margin at constant corrected mass flow, %
T_{45} = total temperature at station 45 (inter-turbine temperature), R°
W_f = fuel flow rate, lbm/s
W_c = corrected mass flow rate, lbm/s

II. Introduction

The aviation community's objectives of reducing the environmental impact of aircraft operations and improving the efficiency, performance, and reliability of commercial aircraft have led to electrified aircraft propulsion (EAP) technology becoming a focus for the National Aeronautics and Space Administration's (NASA) Aeronautics Research Mission Directorate and its partners in government, industry, and academia [1, 2, 3]. The push towards electrification covers a wide array of existing and novel aircraft designs for a range of markets and applications, some of which are shown in Fig. 1. Most recently, significant progress has been made by industry in the development of small, all-electric aircraft aimed at short-haul and urban markets. To date, over one hundred of these advanced air mobility vehicles have been proposed and are in various stages of design, test, and certification [4, 5, 6]. However, these vehicles are being designed to create new markets for air transportation and do not address the largest sources of greenhouse gas emissions from the aviation sector, namely the single-aisle and twin-aisle commercial transports that account for more than 90 percent of the global emissions from commercial aircraft [7]. The aircraft that serve these markets cannot be transitioned to all-electric operation in the near future due to the low specific energy offered by current battery technology as compared to hydrocarbon fuels [8] as well as electrical safety issues associated with the operation of high voltage electrical systems in a low-pressure high-altitude environment [9, 10]. In the near term, despite advances in propulsion technology and airframe design, these aircraft (such as the Airbus A320neo and the Boeing 737 MAX series) will continue to be powered primarily by turbomachinery [11, 12]. Fortunately, even if these aircraft are not transitioned to all electric power there are still stepwise improvements that can be obtained through the adoption of hybrid-electric propulsion systems. The integration of motor/generator electric machines (EMs) into the gas turbine engines (GTEs) that power regional, single- and twin-aisle transport aircraft provides additional control, actuation, and energy management opportunities that can improve both the operation of the GTEs and aircraft's propulsive efficiency [13, 14].

Due to the complexity, high performance, and high-energy nature of turbomachinery used for aircraft propulsion, testing these systems is difficult and expensive, requiring extensive analysis and test support hardware or specially modified aircraft. This is especially true for hybridized turbomachinery, which has additional risk associated with the increased complexity and lower technology readiness level (TRL) of hybrid-electric propulsion technology [9]. As a result, testing and validating these systems presents a significant challenge to the engineers and organizations working to develop them. In this situation, real-time simulation and hardware-in-the-loop (HIL) testing are powerful tools that are used to provide additional validation of the technology and increase confidence in the robustness of control algorithms. In the case of electrified turbomachinery, HIL testing can be used to demonstrate the performance and behavior of the electrical components and energy management control algorithms prior to their integration with the turbomachinery, reducing risk carried forward into future testing with real GTEs and eventually real aircraft.

Figure 1. Examples of single-aisle and all-electric transports. Clockwise from top right: Airbus A320neo, Boeing 737 MAX, Wisk Aero Cora, and Joby Aviation S4

In this paper, an advanced control strategy called Turbine Electrified Energy Management (TEEM) [15] is demonstrated and elevated to TRL 3[1] by a HIL test performed at the NASA Electric Aircraft Testbed (NEAT). The TEEM control algorithm demonstrated in these tests takes

[1] Demonstrates part of the TEEM concept in a laboratory environment

advantage of the EMs integrated into the low- and high-pressure spools (LPS and HPS) of an advanced conceptual turbofan engine design by using them to improve the operability of the engine during throttle transients. The HIL test demonstrates the TEEM algorithm using real megawatt-scale EMs and inverter controllers, interacting with the shafts of a simulated GTE. The results from the HIL test are evaluated against pre-test predictions from development models of both the GTE and the NEAT facility.

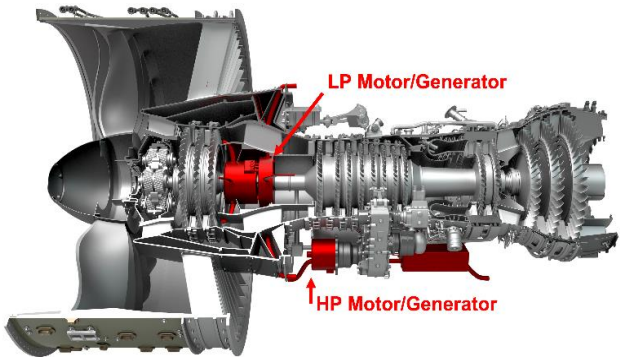

Figure 2. Conceptual hybrid geared turbofan with electric machines on low- and high-pressure spools and supporting hardware shown in red.

The paper is organized in the following manner. A more detailed description of TEEM is provided in Section III. The NEAT facility and real-time emulation system used for the HIL tests are described in Section IV. Key enabling elements of this test were the use of a dynamic power scaling and torque emulation strategy that allowed the turbofan inertial loads to be emulated by the scaled NEAT hardware, as well as the NASA-developed MATLAB/Simulink® modeling tools used to construct the engine and facility models. These tools and strategies are discussed in Section V. The HIL tests involved the real-time engine model and a novel closed loop control and scaling strategy driving the NEAT electro-mechanical system, operating at a representative (megawatt scale) power level. The results of these tests are presented and described in Section VI. Conclusions and recommendations for future work are presented in Section VII.

III. TEEM Background

The TEEM control strategy is an advanced control algorithm that is designed to improve the stability and transient response behavior of a dual-spool GTE by leveraging EMs coupled to one or more of the engine spools [15, 16]. These EMs are included in the design of many hybrid-electric aircraft engine concepts [15, 16, 17, 18] and in most applications may be used primarily for purposes other than TEEM, such as electrical power extraction for driving supplemental electric propulsors, augmenting the GTE during parallel-hybrid operation, or enabling new capabilities such as electric taxi [8, 19, 20]. Figure 2 shows a concept rendering of a hybrid geared turbofan engine with TEEM capability. When designing GTEs, a significant amount of margin is required to ensure that the turbomachinery components, specifically the high- and low-pressure compressors (HPC and LPC), do not exceed stall or surge when moving between steady state operating points [21]. This allowance is referred to as the transient stack and is a portion of the engine's overall stall (or surge) margin (SM). The remainder of this margin is the uncertainty stack, and accounts for uncertainties in the engine's steady state operation such as component degradation and engine-to-engine variation [22]. For the purposes of this paper, SM is defined as the percent difference between the compressor pressure ratio and the stall pressure ratio at a constant corrected mass flow rate, W_c [23]. Figure 3 shows an example compressor map with the stall boundary, SM, and steady state operating lines labeled. This requirement to maintain sufficient SM can constrain the engine capability, particularly during acceleration and deceleration transients [16, 23]. Part of the challenge in maintaining SM is that GTEs have no means of directly applying torque to control their shaft speeds, relying instead on indirect actuation methods such as fuel flow, secondary airflows, and aerodynamic coupling within the engine gas paths to provide the torque necessary for changing speed. Furthermore, the engine spools have different moments of inertia, causing their speed responses to lag the control inputs and leading to divergence from the steady state operating points due to misalignment between the gas path flows and shaft speeds. This misalignment can move one or both of the compressors toward their stall/surge boundary. The high actuation bandwidth of EMs and the fact that they are mechanically connected to the shafts enables a controller to directly affect the shaft speeds. Even if the EMs only contribute a fraction of the overall shaft power, they are

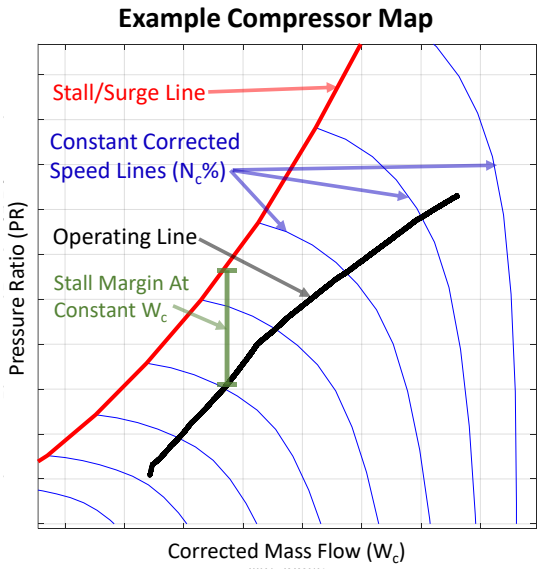

Figure 3. Labeled sample compressor map illustrating operating line and stall boundary

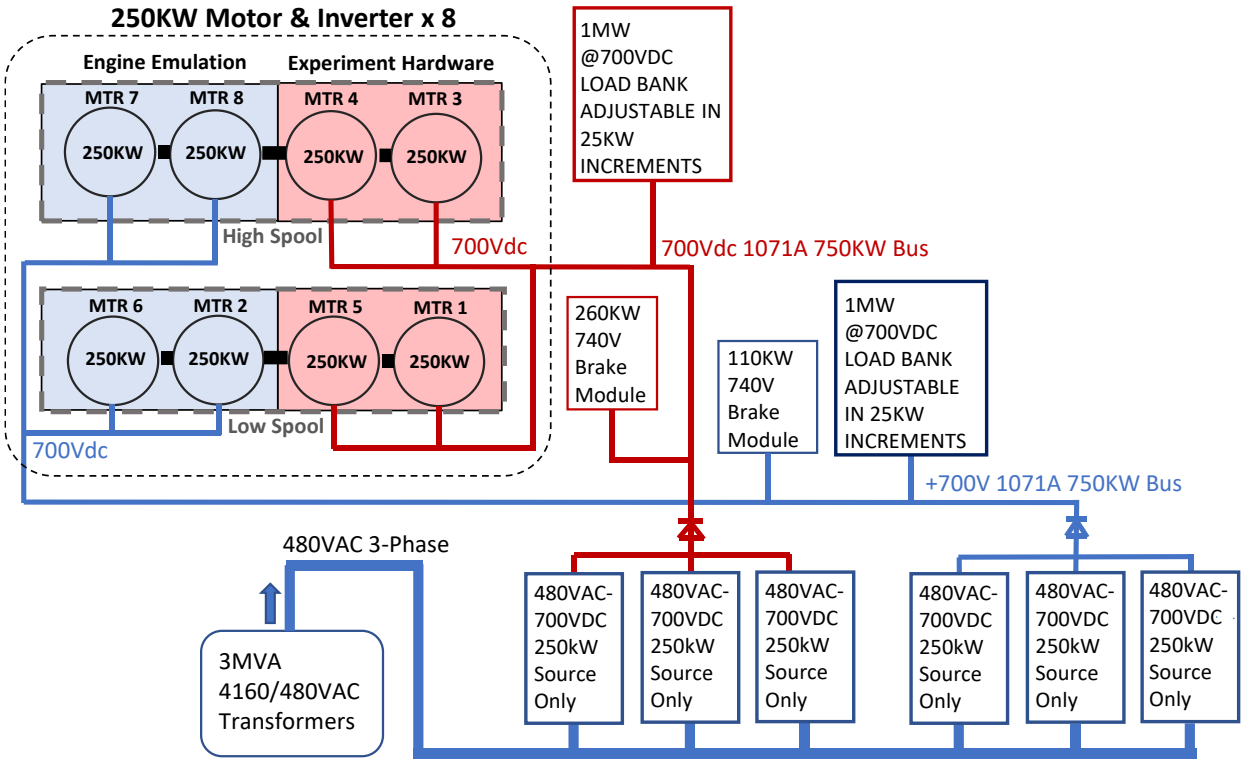

Figure 4. Block diagram showing the configuration of the NEAT facility for TEEM HIL testing

still able to positively influence the operating point of the engine [24, 25]. More information on the formulation and improvement of the TEEM concept and its applications can be found in Refs. [15, 16, 24, 25, 26].

IV. Test Facility

The NEAT facility is located at the NASA Glenn Research Center Neil A. Armstrong Test Facility (ATF) in Sandusky, Ohio. NEAT is designed as a reconfigurable testbed capable of testing megawatt-scale electro-mechanical EAP systems at full-scale power and altitude conditions. The facility can accept up to 24 MW of electrical power and operate as high as 4500 volts DC [9, 10]. In this test configuration, NEAT supplies up to 1.5 MW of electrical power at 700 VDC, which is sufficient to represent the sub-scale hybridized turbofan engine and TEEM power system. For the TEEM tests, NEAT is set up to emulate the shaft dynamics of an advanced geared turbofan engine with EMs on both the low-pressure and high-pressure spools (LPS and HPS). This engine is described in more detail in Section V.

The NEAT facility hardware layout for the TEEM tests, illustrated in Fig. 4, consists of eight 250 kW permanent magnet synchronous motors (PMSMs) set up on two separate shafts, four PMSMs to a shaft (designated MTR 1 through MTR8). These shafts are used as dynamometers in other NEAT applications [9]. Each PMSM is controlled by a matching inverter and operates on 3-phase AC power. Two PMSMs on each shaft are connected to a common DC bus, with the other two on each shaft connected to a second, separate DC bus (illustrated as blue and red buses in Fig. 4). The research/experiment bus and associated PMSMs (in red) represent the electro-mechanical hardware integrated into the hybridized turbofan, specifically the LPS and HPS EMs and motor controllers. The emulation bus (in blue) is used to power the PMSMs that represent the turbofan engine and emulate the scaled dynamic speed and torque responses of the engine shafts to the torques from the experiment side. Each DC bus is powered by three 250 kW unidirectional power supplies (750 kW per bus) connected in parallel, which are used to regulate the buses to 700 VDC. Brake resistor banks connected to each bus can reduce the bus voltage if it exceeds 740 V. Each bus is also connected to a separate reconfigurable resistive load bank, adjustable in 25 kW increments up to 1 MW. The facility can sink up to 2 MW of power through these load banks.

A detailed diagram of the real-time simulation and communications setup used for the TEEM testing is shown in Fig. 5. The turbofan engine model is run on a dSPACE SCALEXIO® real-time computing system and controlled by an industrial PC desktop computer. The engine model was created in the MATLAB/Simulink environment and converted to a real-time application. The system is controlled using a custom graphical user interface (GUI), which is also used to collect and store telemetry from the inverters, send commands to the real-time application, and edit test-

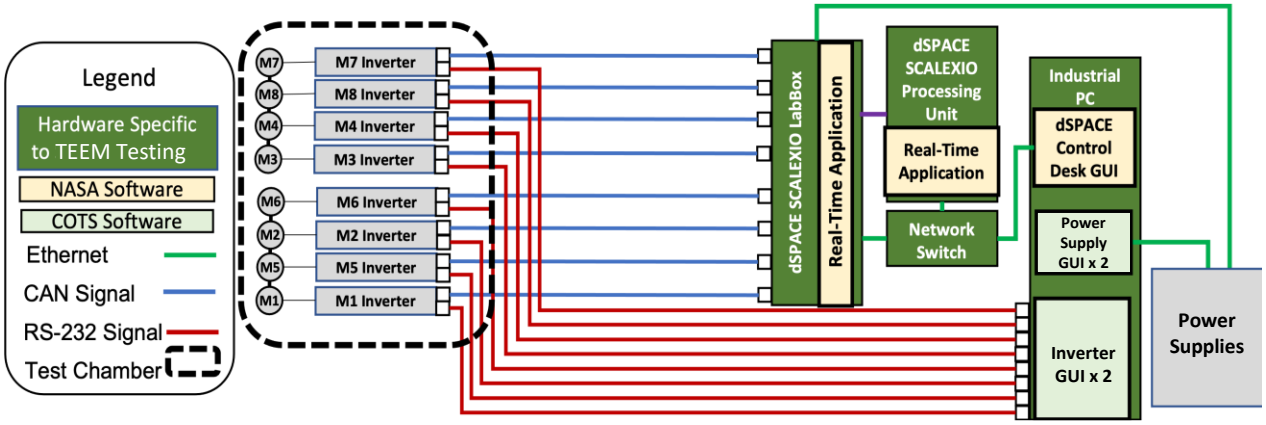

Figure 5. NEAT Simulation and Communications Configuration

specific settings. Inverter telemetry includes speed and torque feedback, AC and DC voltage and current measurements, and temperature data. The real-time computer communicates directly with the inverters over a Controller Area Network (CAN) bus connection. Independent measurement data were collected by a multi-channel data acquisition system (DAQ) that recorded separate speed, temperature, current, and voltage data as well as facility health parameters such as vibration levels, motor temperatures, and cooling flows.

V. Engine and Facility Modeling

The HIL TEEM testing at NEAT requires the use of a real-time turbofan engine model to drive the emulation of the dynamic response of the engine to the shaft EM actuator torques. For this purpose, a well understood NASA-developed model of an advanced turbofan engine is selected. The engine is modified to include an electric power system (i.e., EMs on both engine shafts), and is used to test the implementation of the TEEM algorithm. This engine model is referred to as the Software-in-the-Loop (SIL) model and is used to create a predicted performance baseline for the real-time engine model in the HIL test. The SIL engine model is then combined with the novel test-enabling closed loop emulation and scaling algorithm and a simplified electrical power system model of the NEAT facility as configured for TEEM testing. This combined engine and facility model is referred to as the simulated hardware-in-the-loop (SHIL) model and is used to test the interface between the engine model and the NEAT facility, as well as to predict the emulation controller and facility behavior. For the HIL tests, the SHIL engine model and emulation controller are converted into a real-time application and the EMTAT facility model is replaced with the NEAT hardware. The AGTF30 shaft responses are emulated by the NEAT PMSMs on the emulation bus. A further discussion of the engine model, facility model, and emulation and scaling strategy is held in the following subsections.

A. AGTF30 Engine Model

The Advanced Geared Turbofan - 30,000 lbf (AGTF30) is a conceptual advanced commercial transport turbofan engine model in the 30,000 lbf thrust class. For this test, the AGTF30 was modified to enable TEEM through the addition of an electrical power system model and a transient control algorithm. The AGTF30 engine model was originally created by NASA Glenn Research Center as a reference design for an advanced turbofan and is intended to be representative of commercial engines expected to enter into service in the 2030 -2035 (N+3) timeframe [27, 28]. It is a geared turbofan that has reduced thrust-specific fuel consumption (TSFC) compared to modern turbofans, enabled by an ultra-high bypass ratio, a compact core with a high compressor overall pressure ratio and hotter than usual turbine inlet temperature. Other advances include the fan gearbox, enabling the larger fan to operate more efficiently, as well as the inclusion of a variable area fan nozzle (VAFN) to improve fan operability and a variable bleed valve (VBV) to improve the stability, i.e., SM, of the LPC. For the purposes of TEEM testing, the AGTF30 was modified to include EMs connected directly to both the low- and high-pressure shafts. The LPS EM is rated at 410 hp and the HPS EM is rated at 750 hp, based on a sizing study performed in Ref. [24]. Figure 6 shows a block diagram of the AGTF30 layout and actuators. For the TEEM HIL tests, the EMs and controllers are implemented in hardware as the NEAT PMSMs and their inverter controllers. The energy storage/management block is represented by the unidirectional power supplies and load banks.

Two separate engine controllers are used during the HIL tests to illustrate the performance of the AGTF30 with and without TEEM control. These controllers are built into the AGTF30 Simulink model for the SIL and SHIL testing and are converted with the engine model to the real-time application for the HIL tests. The controller without TEEM control (referred to as the baseline controller) does not utilize the EM actuators on the LPS and HPS. It uses a closed-loop gain-scheduled proportional-integral (PI) controller to regulate the fuel flow, *Wf*, to control to a corrected fan shaft speed N_{1c}. The set-point N_{1c} is determined based on the commanded power lever angle (PLA), altitude, and Mach number (MN). PLA is the physical angle of the engine throttle, and correlates roughly linearly with engine thrust. The PLA ranges from 40° at idle to 80° at maximum power. The fuel flow controller includes several limit controllers to protect against steady-state parameter limit violations such as inter-turbine temperature (T_{45}) and HPC static discharge pressure (P_3), as well as to guard against compressor surge and stall during accelerations and decelerations. The VBV and VAFN operate on fixed schedules based on MN, *N1c*, and LPS EM torque. The controller utilizing the TEEM algorithm (referred to as the TEEM controller) uses the same fundamental scheduled PI *Wf* control and steady state limits. The primary differences are the use of the EM actuators and a simplified set of acceleration schedules for the limit controllers. The EM actuators are applied to suppress transient excursions that reduce compressor stability by directly applying torque to the HPS and LPS when there is a large disagreement between the commanded and sensed active control variable of the fuel flow rate controller. This is typically the N_{1c} error but could also be a limiter such as T_{45} or P_3. Activation/deactivation logic is present to assure that the off-nominal torques are only applied during transients. The TEEM controller usually calls for adding power to the HPS during accelerations, while during decelerations it is advantageous to extract power from the LPS and/or add power to the HPS. Further details on the AGTF30 baseline and TEEM controllers are found in Refs. [15, 24, 16].

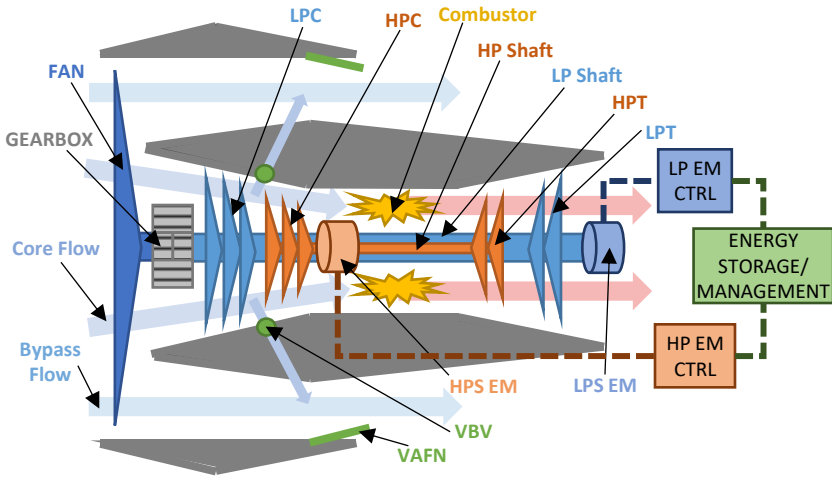

Figure 6. Block diagram showing the notional layout of the AGTF30 hybrid geared turbofan engine with EMs integrated into both spools

The AGTF30 engine model is implemented in the MATLAB/Simulink environment using the Toolbox for Modeling and Analysis of Thermodynamic Systems (T-MATS) [29]. T-MATS is a non-linear zero dimensional aero-thermal modelling tool that uses performance maps to determine the behavior of the turbomachinery system at each simulation timestep. For simplicity, heat soak and other second-order engine temperature effects are not included. The T-MATS solver is set to a fixed, 15 millisecond timestep that is also used throughout the real-time system model. The AGTF30 T-MATS/Simulink model is used in the SIL and SHIL models. To create the real-time engine model used in the HIL tests, the Simulink model was converted using the Simulink coder to an executable hosted on a real-time target using the dSPACE ControlDesk® experiment software.

B. NEAT Facility Electrical Model

For the SHIL pre-test predictions, the AGTF30 electrical system (i.e., LPS EM and HPS EM) and the NEAT facility hardware were modeled using the PowerFlow blockset of the Electrical Modeling and Thermal Analysis Toolbox (EMTAT) [30]. The component based EMTAT model uses simple efficiency tables to predict the voltage, current, and power losses for each component in the power system at a fidelity compatible with the real-time turbomachinery model. Rapid electrical transients are neglected as they occur on timescales far shorter than turbomachinery dynamics. White noise is injected into the simulated feedback signals to test the robustness of the emulation and engine model controllers. The SHIL EMTAT facility model is used to test the power scaling and emulation controller discussed in the following section, predict the electrical power required for each test case so the load banks could be set accordingly, and to confirm the team's understanding of the behavior of the electrical system. For the HIL tests, this model was replaced with the real NEAT facility electrical hardware.

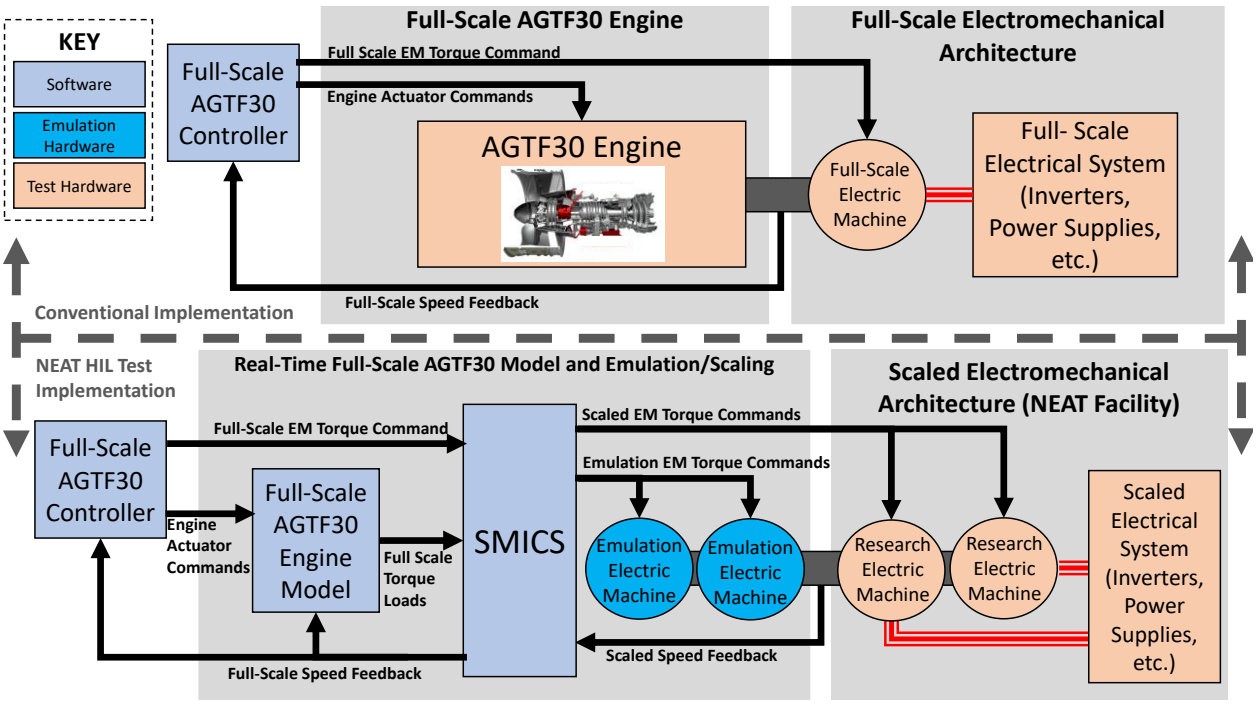

Figure 7. Engine and SMIC emulation controller implementation diagram (showing one shaft/engine spool)

C. Power Scaling and Emulation

A key enabling component of the TEEM testing is the dynamic scaling and emulation controller that allows the torque response of the AGTF30 shafts to be emulated using the NEAT hardware. A specially developed Sliding Mode Impedance Controller with Scaling (SMICS) is used to make the PMSMs on the emulation bus mimic the scaled inertial load of the turbofan in response to the TEEM actuator torques produced by the experiment-side hardware [31, 32]. Closed-loop control is implemented around the facility shaft speeds. A diagram of the engine model and closed-loop hardware control with SMICS is shown for one shaft in Fig. 7, and is compared to a more conventional turbomachinery HIL test configuration where the EMs are connected to a real engine. The torque commands sent to the engine EMs for TEEM are scaled linearly by the SMICS block before being passed to the experiment-side EMs, while the sliding mode impedance control portion of the algorithm sends torque commands to the emulation-side EMs to control the shaft speed and mimic the torque response of the engine shafts. The shaft rotational speeds need to be scaled down to meet the speed constraints of the NEAT hardware, while the torque from the LP EM, HP EM, and emulation motors were scaled to match the 500 kW power constraints of the NEAT motors (2x 250 kW PMSMs). The speed feedback signal is also processed through a low-pass filter to aid in noise rejection.

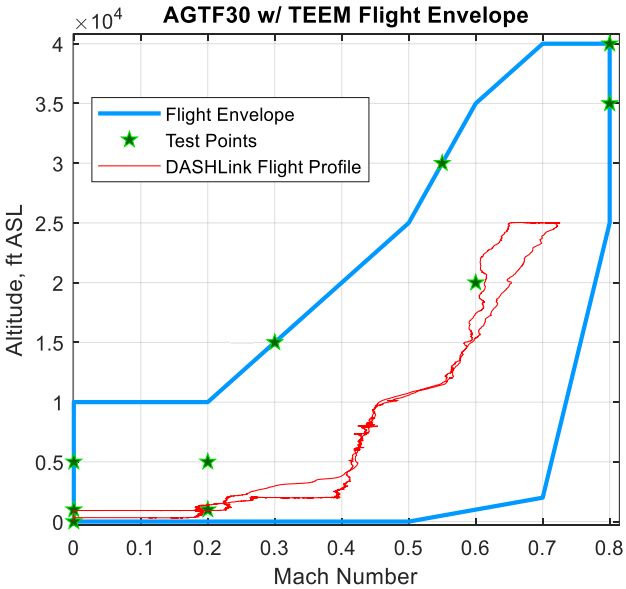

Figure 8. AGTF30 flight envelope including fixed test points a through j, and test suite 6 (full flight profile)

VI. Results Comparison

The HIL testing of the AGTF30 engine model and TEEM controller involved running the AGTF30 through various PLA input profiles at ten different simulated altitude and Mach number conditions throughout the flight envelope. These fixed test points are shown in Fig. 8. There are six total PLA profiles. Profiles 01 through 05 are run at each of the ten fixed

test points to illustrate the performance of the AGTF30 with the baseline and TEEM controllers across the flight envelope. Profile 06 is comprised of altitude, MN, and PLA profiles for a representative 70-minute flight and is used to illustrate the performance of the engine with TEEM control under realistic flight conditions. In this analysis, altitudes are given in feet above mean sea level (ASL). In total, 51 tests totaling 10.1 hours of runtime were run with the NEAT hardware. The appendix contains a brief description of the different throttle profiles and test points as well as the naming conventions used in the rest of this section. The following subsections discuss the results of the HIL tests, which showed close matching between engine state, engine actuator, and facility measurements across the SIL (engine model and controller only), SHIL (engine model and controller with SMICS and EMTAT facility model), and HIL (real-time engine model with SMICS and facility hardware) tests. Due to the large quantity of data collected, the analysis will focus primarily on the full flight profile and the subset of the fixed test points required to illustrate the accuracy of the facility model predictions and the effectiveness of the HIL TEEM control. Data presented in this section are inverter telemetry recorded through the dSPACE system. The independent measurements recorded by the DAQ system were used to verify the inverter measurements but for brevity's sake are not presented here.

A. NEAT Facility Data

Results from the SHIL facility model and HIL tests are shown in Fig. 9. To quantify the accuracy of the pre-test predictions the relative errors between several of the simulated and measured parameters from the SHIL and HIL results are shown in Table 1. The error is calculated for two separate test cards: test card 03a (snap throttle transients at sea-level-static (SLS), baseline controller) and test card 05a (snap throttle transients at sea-level-static (SLS), TEEM controller). Profiles are referred to as "snap" transients because the PLA command switches between reference points over one 15ms timestep. These test cards are selected because they demonstrate the matching between the predicted and measured EM performance for both the baseline controller and TEEM controllers across a range of power levels

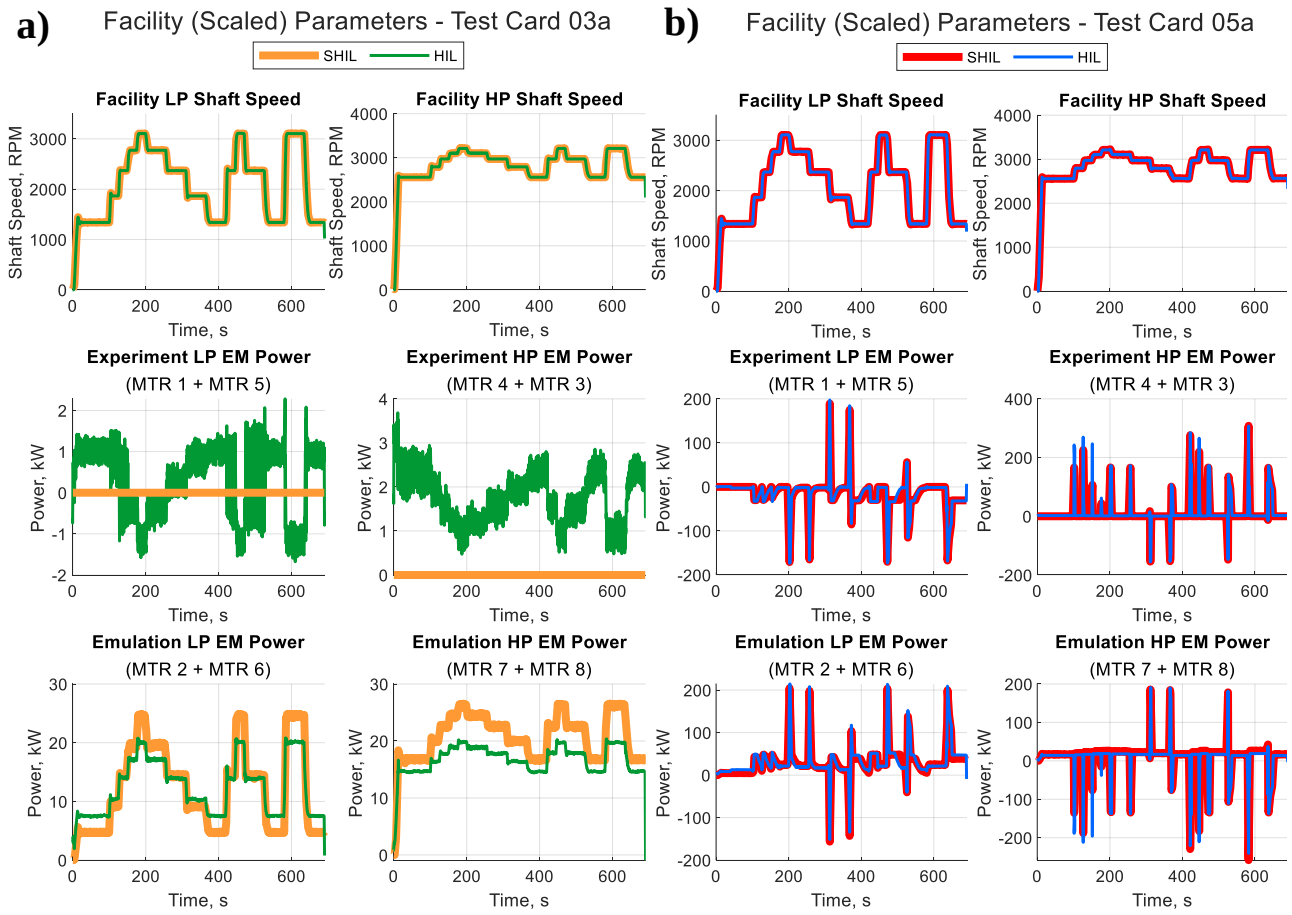

Figure 9. SHIL predictions and HIL test results for snap PLA profiles at SLS: (a) Test Card 03a (baseline controller) and (b) Test Card 05a (TEEM controller). The experiment side EM powers in (a) represent electrical noise in the system due to the free spinning PMSMs not being used by the baseline controller.

for the most aggressive PLA movements. The relative error is calculated as a root-mean-square relative error (RMSRE) between the pre-test SHIL prediction and the measured HIL results. The RMSRE for each measurement is normalized by the magnitude of the maximum predicted value for that parameter (from the SHIL model). The effects of the different noise signatures between the SHIL simulation and HIL measured results are handled by smoothing the data with a locally weighted regression using a span equivalent to 1 second at the signal's sample rate (67x 15ms timesteps or 1000x 1ms timesteps). For the EM power calculations, the DC voltage and current recorded by the inverters were multiplied to get the electrical power. The power for each pair of two EMs was calculated separately and then summed.

Table 1. Normalized RMSRE between SHIL and HIL results

	Normalized Root Mean Squared Relative Error (RMSRE) (%)	
Facility Parameter	**Test Card 03a (No TEEM)**	**Test Card 05a (TEEM)**
Scaled LPS Speed	0.06%	0.11%
Scaled HPS Speed	0.06%	0.07%
LPS Experiment EM Power	N/A*	2.26%
HPS Experiment EM Power	N/A*	3.13%
LPS Emulation EM Power	10.39%	3.31%
HPS Emulation EM Power	16.27%	3.70%

* SHIL data was not collected for experiment motors for test suites 1, 2, and 3 as the TEEM actuators were not used

For all cases, the shaft speeds match very closely between the SHIL and HIL models, with RMSREs close to one tenth of a percent in Table 1 and excellent agreement shown in Fig. 9. This is because the closed-loop SMICS is working to drive the scaled shaft speed error to zero and illustrates the effectiveness of the emulation controller. At low EM powers (less than 10% of the rated power) like the ones shown for the EM power plots in Fig. 9a, it can be seen that the SHIL predictions for the emulation controller diverge significantly from the measured values. This divergence is likely due to poor estimation of the PMSM and inverter efficiency maps used in the EMTAT components in the SHIL model. Specifically, it was observed that the viscous damping on the NEAT dynamometer shafts was nonlinear and difficult to predict. This unmodeled effect significantly affected the test cards where there was little or no torque applied by the experiment side EMs (i.e. tests where TEEM was not used), leading to RMSREs over 16% in Table 1. For test cards where higher power was required from the EMs to emulate the shafts and the experiment side machines, the viscous damping effect accounted for a smaller portion of the overall power, leading to RMSREs below 4% in Table 1 and leading to much better qualitative matching in Fig. 9b. A source of the remaining error in the EM power is likely the fact that the lower-fidelity EMTAT model does not adequately capture the transient electro-mechanical dynamics of the PMSMs, which were modeled simply as an inertial load when not powered, or the inverter controllers, which were controlling the motor torque via an internal PID current loop. Differences in sensor noise could also contribute to the remaining error. The SHIL model used white noise to test the low-pass filter and SMICS noise/disturbance rejection, however the test data showed that at certain shaft speeds, lower frequency (>2 Hz) oscillations could start to affect the real-time model, leading to minor deviances in the response of the SMICS. Despite these imperfections, the EMTAT based SHIL model still accurately predicted the dynamometer behavior and power requirements for the NEAT HIL test.

B. Engine Model Data

In order to demonstrate the close matching between the predicted SIL and measured HIL test results, RMSREs and plots of the AGTF30 engine performance are shown in Table 2 and Fig. 10 respectively. For the engine parameters, the discussion focuses on the full flight profile as it offers a more realistic set of environmental and control inputs than the PLA steps from the previous section. The flight is divided into three portions, based on the rate of climb in the simulated profile: takeoff/climb, cruise, and descent/landing. A detail of the profile is given in the appendix. The sensed parameters *N2*, *N3*, *T45*, and *Ps3* are used by the AGTF30 baseline and TEEM controllers, while the compressor SMs are used to illustrate the system stability and net thrust (*Fnet*) is used to illustrate overall performance. As with the

Table 2. Normalized RMSRE between SIL and HIL test results for engine sensed parameters, actuators, and stability margins

Engine Parameter	RMSRE for Phase of Flight		
	Climb	**Cruise**	**Descent**
LPS Speed (N_2)	0.04%	0.04%	0.64%
HPS Speed (N_3)	0.02%	0.06%	0.25%
Wf Actuator	0.16%	0.22%	1.19%
T45 Sensed	0.07%	0.12%	0.51%
Pt3 Sensed	0.10%	0.10%	1.07%
Fnet	0.14%	0.13%	1.20%
LPC SM	0.19%	0.20%	1.22%
HPC SM	0.24%	0.47%	0.75%

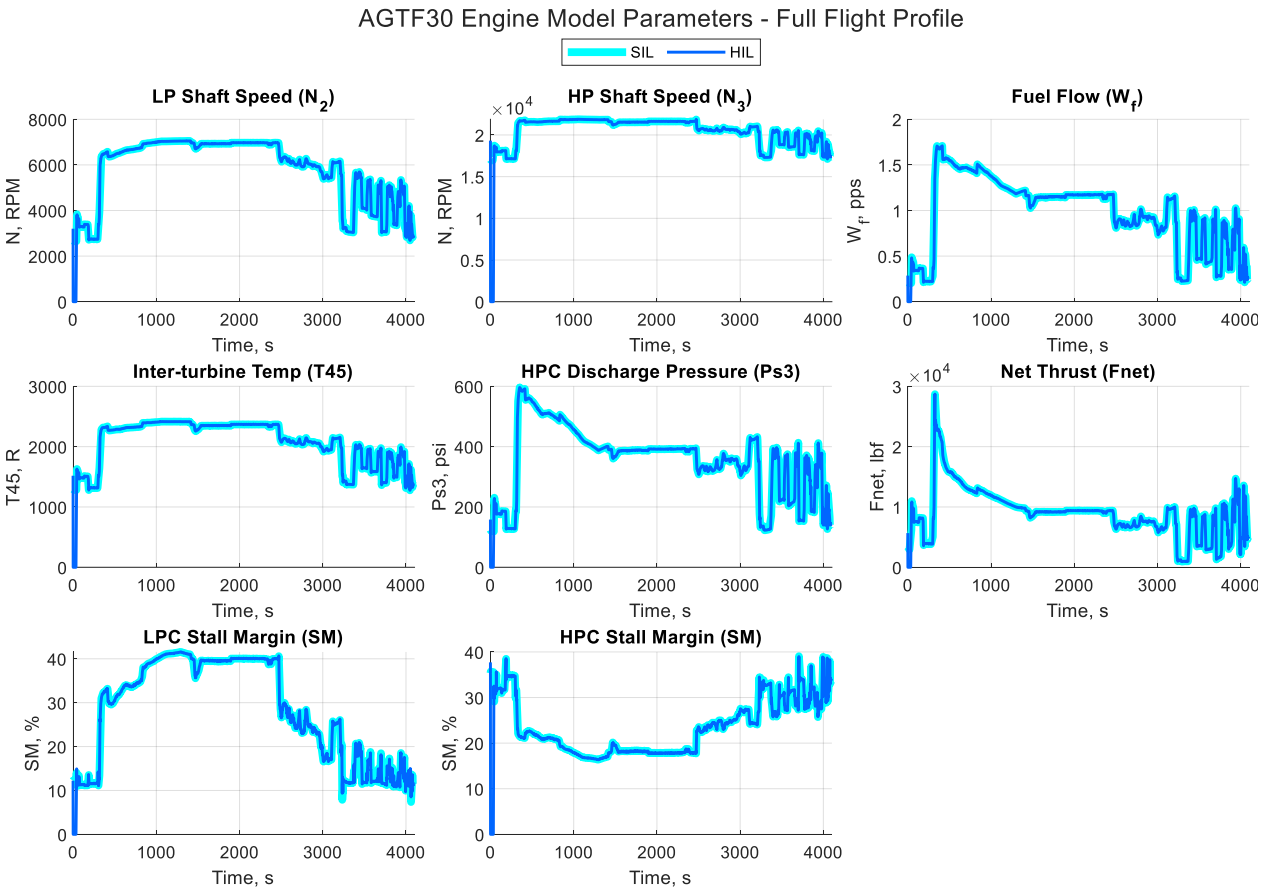

Figure 10. Test results comparison for the full flight profile. The climb portion runs from 350 to 1300 seconds, and the descent portion runs from 2500 to 4000 seconds. The altitude, MN, and PLA profiles from Ref. *[34]* **are highlighted in the appendix**

facility data the results are smoothed with the same locally weighted regression before calculating RMSRE and the errors are normalized by the maximum predicted SIL value for each parameter. From Table 2, the matching between the pre-test SIL and HIL results is closer than for the facility parameters in test cards 03a and 05a, with no parameter exceeding 1.25% RMSRE. A reason for this is that the engine model only uses the shaft speeds to determine the thermodynamic properties of the gas path. Thus, differences between the predicted and measured EM power and torques are attenuated by the shaft inertias and passed through the SMICS controller before being seen by the engine model. The descent portion of the flight was the most difficult to match, as it contains a rapid series of transients that were more affected by the NEAT facility damping and electrical characteristics. Figure 10 also shows the qualitative matching between each parameter during the climb and descent portions of the flight profile. The higher errors in the descent phase are likely due to the increase in PLA movements between 3000 and 4000 seconds, leading to the differences predicted and observed transient behavior mentioned before.

C. TEEM Performance Benefits

A goal of the work effort covered in this paper was to demonstrate TEEM on a scaled electro-mechanical system, and to verify that real sensor and actuator constraints do not significantly diminish the capability of the TEEM controller to improve engine operability. Without a physical GTE to test, the engine operability and performance is still captured using the real-time AGTF30 model. However, the shaft speeds and EM torques used by the model are supplied by the NEAT hardware, which both emulates the engine shafts and represents the scaled TEEM electro-mechanical hardware. This configuration allows real-world factors that can negatively affect control algorithms such as torque ramp rate limits, sensor bias and noise, and inverter controller tuning to be included [21]. To evaluate the impact of the real actuator hardware on the TEEM controller, detailed engine parameter results are shown for the throttle burst/chop movement at the end of PLA profiles 03 (baseline controller) and 05 (TEEM controller) at SLS

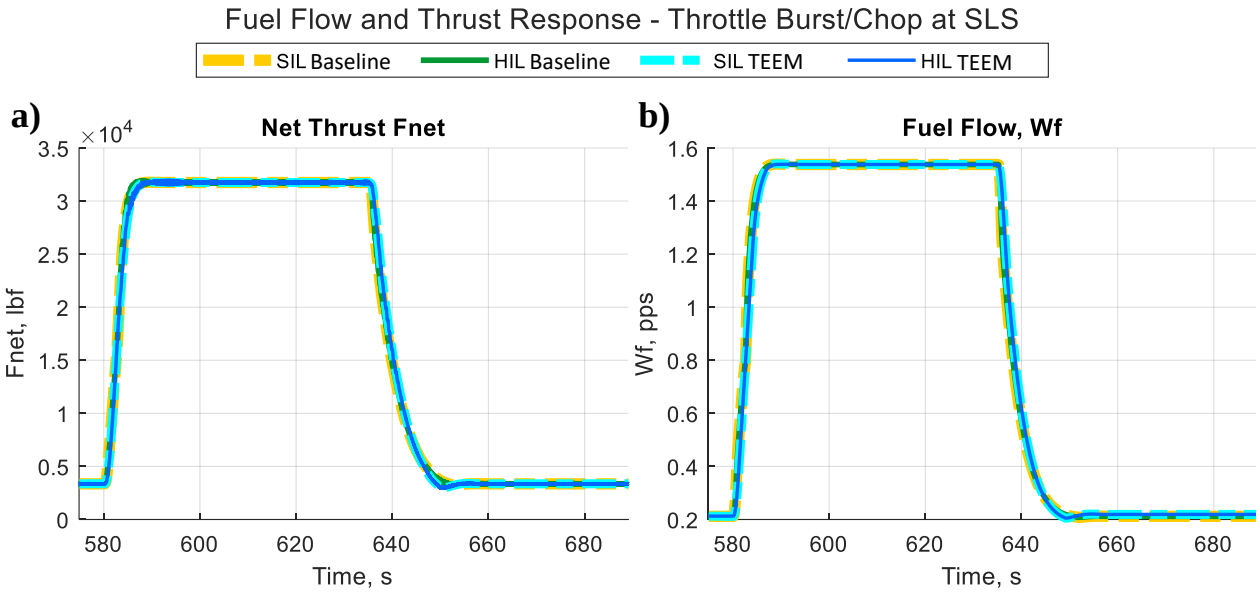

Figure 11. (a) AGTF30 Thrust Response and (b) Fuel Flow Command for a burst/chop throttle transient with baseline and TEEM controllers

conditions (test point a: altitude = 0 ft ASL, MN = 0). The burst/chop is an aggressive throttle movement from idle to full power and back, and is used as a stress test for the model and controller. These results are selected because they represent the most aggressive test of the TEEM controller, and because at high altitudes the simplified acceleration schedules used by the TEEM controllers [15] make it difficult to isolate the effects of the TEEM actuators as compared to the baseline controller. Both SIL and HIL engine data is presented to demonstrate that the observed behavior of the AGTF30 with the TEEM controller matched the predictions from the original model.

Figure 11 shows the net thrust response (a) and fuel flow actuator (b) for the burst/chop from test cards 03a and 05a. The thrust response from both controllers is the same for acceleration and deceleration, allowing the effects of the TEEM controller to be isolated. The similar steady-state thrust, response time, and overshoot represent the same level of engine performance as observed from the aircraft and pilot's perspective. Just like the results in Fig. 10, both the *Wf* and *Fnet* results from the real-time engine tests were accurately predicted by the SIL T-MATS model. The EM actuator outputs commanded by the TEEM controller are shown in Fig. 12 at the same SLS conditions. These are the

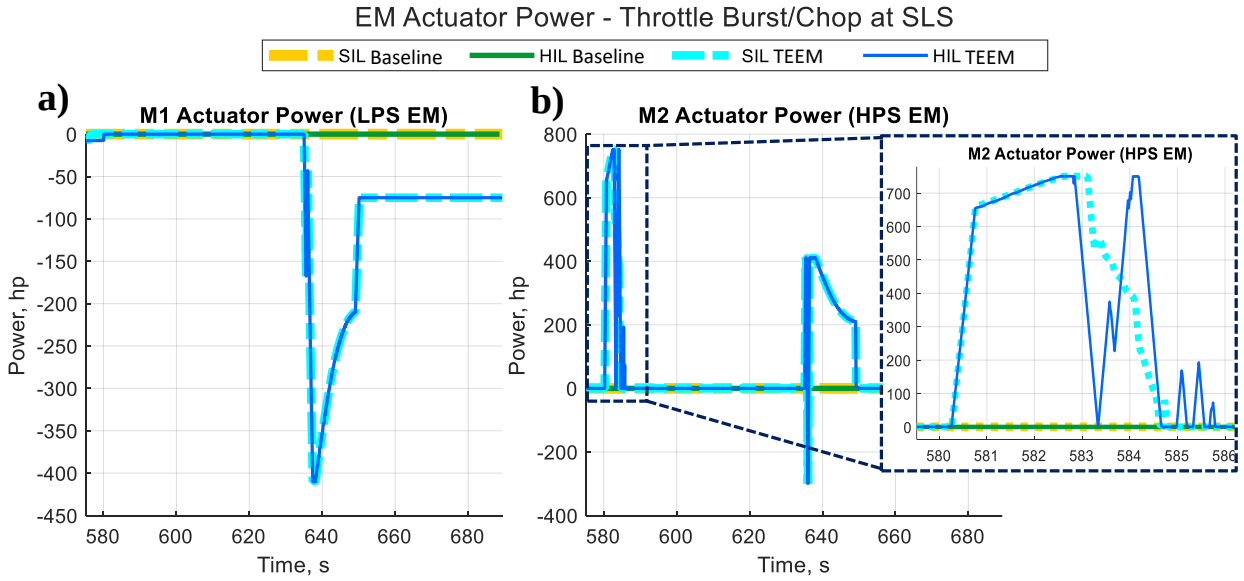

Figure 12. AGTF30 EM Actuators: (a) M1 – LPS EM and (b) M2 – HPS EM with inset detail of actuator power during the deceleration transient

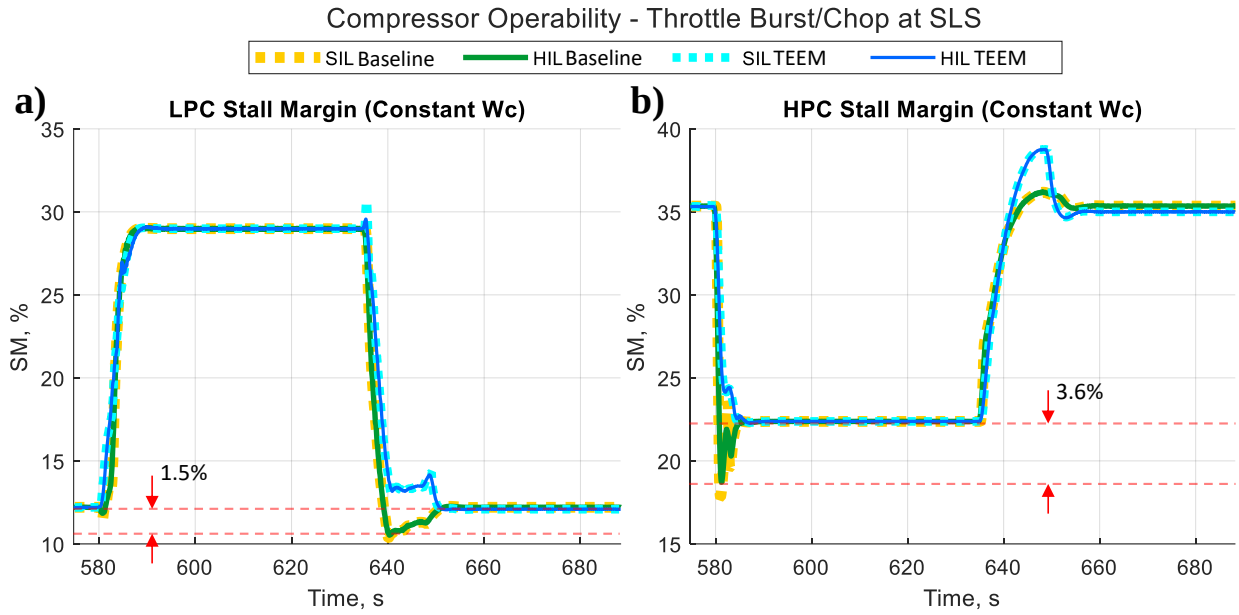

Figure 13. AGTF30 LPC (a) and HPC (b) Stall Margins. Minimum margins with and without TEEM are highlighted, illustrating the observed SM benefits

mechanical power outputs of the HPS and LPS EMs as seen by the AGTF30 engine shafts. The EM actuator commands are zero when using the baseline controller (test card 03a). As can be seen in Fig. 12a and 12b, for points when TEEM control is active, the SIL predictions for the EM outputs from both the LPS and HPS (M1 and M2 respectively) closely match the HIL results. There are some minor discrepancies toward the end of the acceleration transient for the M2 actuator, highlighted in the inset in Fig. 12. This disagreement could be due to small fluctuations in the NEAT shaft speed measurement as the set-point is approached. As the sensed value approaches the set-point, the sign of the error used in the SMICS flips back and forth and cause it to chatter (a known feature in sliding-mode control). This chatter could be exacerbated by the relatively large 15ms timestep and the low inertia of the NEAT dynamometer system that the SMICS uses to mimic the dynamic response of the significantly larger turbofan, leading to imperfect damping of such oscillations. As mentioned in the previous subsection, other data artifacts relating to shaft speed measurement noise were able to affect the real-time model. For future work, retuning of the SMICS and improved feedback signal filtering may minimize these effects. However, the observed discrepancies occur only over very short time periods and do not significantly impact the operability of the AGTF30 engine model or the net power delivered by the M2 actuator. Note that the sustained non-zero power extraction with the LPS EM toward the end of the test segments represents power used for re-charging the energy storage device that would exist in the power system, in this test it gets bled off through the load banks.

Figure 13 shows the LPC SM and HPC SM for the same burst chop at SLS. For both compressors an improvement in minimum SM is apparent. Quantitatively, using the HIL results from the TEEM controller the HPC gains 3.6% SM on the acceleration and the LPC gains 1.5% during the deceleration transient, all while delivering the same thrust response and fuel consumption as the baseline controller. It should be highlighted that these SM benefits align with those predicted by the original formulation of the TEEM control concept when applied to a different NASA developed conceptual hybrid-electric turbofan, which demonstrated a 2.2% HPC SM gain and a 4.3% LPC SM gain [16]. The results also show excellent agreement between the SIL predictions and the HIL results, reinforcing the TEEM controller's ability to use the test hardware EM actuators to influence the engine model and achieve the desired effects on the engine operability.

The effect of the TEEM controller can also be illustrated by looking at the compressor maps during the same burst/chop transient (Fig. 14). The maps show how TEEM moves the compressor operating points further away from the stall line during the duration of the transients, as compared to the baseline controller. The key subsections of this figure are Fig. 14b, which shows the HPC SM gain during acceleration, and Fig. 14c which shows the LPC SM gain during deceleration. The A smoothing function with a locally weighted regression and a window equivalent to 1 second, similar to the function used to smooth results for the RMSRE calculation, is used to minimize the noise and improve the readability of the maps. This noise, also somewhat visible in the SM plots in Fig. 13, is likely due to the observed oscillation in the shaft speed signals and the nature of the zero-dimensional propulsion model. Because the

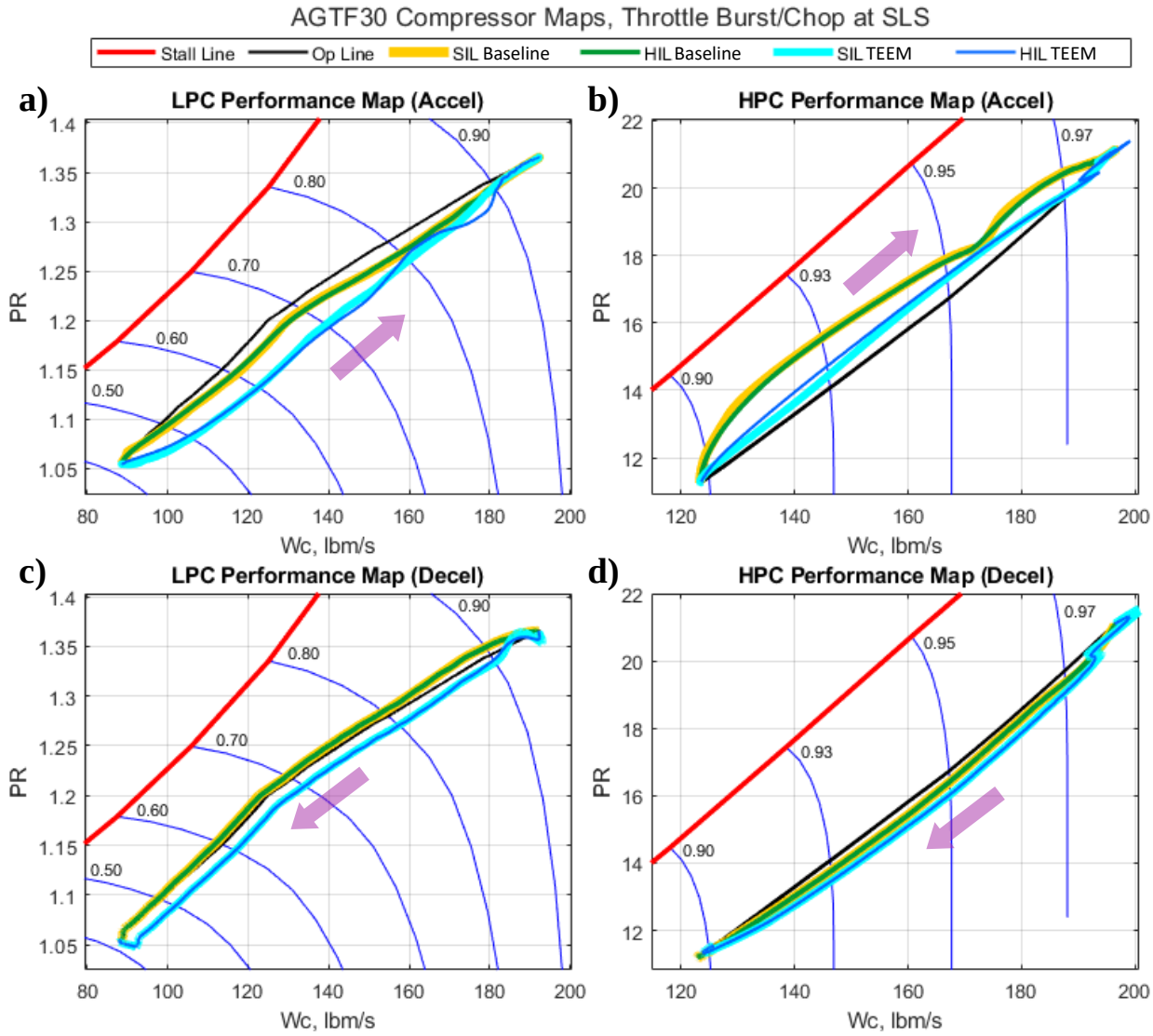

Figure 14. AGTF30 Compressor Performance Maps: LPC burst (a) and chop (c) and HPC burst (b) and chop (d) at SLS. Baseline controller is in green/yellow, TEEM controller is in blue/cyan. Stall/surge line and steady state operating line are called out. Blue arcs represent constant speed lines in % of max *Nc*. Purple arrows indicate direction of motion on map.

operability of the compressors is a function of shaft speed and the model lacks time-dependent flow constraints such as fluid transport continuity, this oscillation is likely non-physical and is a factor of the model only. This inconsistency can explain the momentary divergence of the SIL and HIL results at the end of the acceleration transient (PLA burst). However, with regards to stability limits and overall compressor performance, the maps reinforce the accuracy of the SIL pre-test predictions and the ability of TEEM to successfully affect the operability of the real-time engine model using the megawatt-scale NEAT hardware.

VII. Conclusions

The results of the Turbine Electrified Energy Management (TEEM) hardware-in-the-loop (HIL) tests conducted at the NASA Electric Aircraft Testbed (NEAT) show excellent agreement between the modeled pre-test predictions and the measured results from the electro-mechanical testbed. The use of the novel sliding mode impedance controller with scaling (SMICS) allowed the real-time turbomachinery system to be successfully scaled and emulated by the megawatt-scale NEAT hardware. The software-in-the-loop (SIL) and simulated hardware-in-the-loop (SHIL) Advanced Geared Turbofan – 30,000 lbf (AGTF30) engine and NEAT facility models successfully predicted the

behavior of both the NEAT electro-mechanical hardware systems and the real-time engine model during the HIL testing. The TEEM controller was able to influence the operability of the engine model through the use of real electromechanical actuators and increase the stability margins of the low- and high-pressure compressors (LPC and HPC), achieving performance benefits similar to those predicted by previous analysis. Slight variations in the TEEM commands between SIL and HIL results are observed and are likely due to unmodeled shaft damping effects and unfiltered fluctuations in the feedback signals to the SMICS emulation controller, however these differences have negligible effects on the overall simulated engine behavior. Additional hardware characterization and validation of the component models could be used to mitigate these effects in future tests. These results, along with a complementary set of tests performed on NASA's Hybrid Propulsion Emulation Rig (HyPER) testbed [33], raise the TEEM algorithm to technology readiness level (TRL) 3 by demonstrating the success of the control strategy with real actuators in a laboratory environment. The tests also increase confidence in the ability of the Electrical Modeling and Thermal Analysis Toolbox (EMTAT) PowerFlow modeling tools to predict the behavior of the electromechanical system on the turbomachinery timescales and demonstrate the utility of the Toolbox for Modeling and Analysis of Thermodynamic Systems (T-MATS) for creating engine models for real-time applications. Future work should leverage the risk reduction achieved by the HIL tests and move forward with testing TEEM algorithm on real turbomachinery systems. The NEAT and HyPER testbeds can also be leveraged for additional studies to refine the TEEM algorithm and apply it to other electrified aircraft propulsion (EAP) systems.

Appendix

This appendix contains a summary of all the tests run during the AGTF30/TEEM testing campaign at NEAT. The term "test card" is used to refer to a single test, while "test suite" refers to a collection of test cards. For test suites 01 through 05, a single PLA profile was run at 10 fixed simulated altitude and Mach number settings (designated "a" through "j" and listed in Table A-1). Each PLA profile was run at each test point, resulting in the naming convention "Test Card [Throttle Profile][Test Point]." As an example, the designation "Test Card 05a" refers to throttle profile 05 run at Test Point "a". Figure A-1 shows the PLA profiles with brief descriptions of each test suite. Test suite 6 involved running the engine through a 70-minute simulated full-flight profile [34], referred to as Test Card 06a, which uses sample flight data from NASA's Discovery in Aeronautics Systems Health (DASHlink) website. The throttle, altitude, and MN inputs for this test are shown in Fig. A-2. Altitudes are given in feet above mean sea level (ASL). Test cards 03a, 05a, and 06a are presented in detail in the body of the paper. PLA profile 01 was used to verify the steady-state performance of the AGTF30 across a range of power levels. Profiles 02 and 04 are throttle ramps and are used to establish a baseline for transient performance for the AGTF30 with both the baseline and TEEM controllers at a variety of power settings. Profiles 03 and 05 are rapid "snap" throttle transients where the PLA command changes setpoints over one 15ms model timestep. These profiles are used as a stress test of the baseline and TEEM controllers. The full flight profile exposes the hybrid turbofan engine and the TEEM controller to a realistic set of transients across the entire flight envelope, including simultaneously changing altitude, MN, and PLA.

Table A-1. Fixed Flight Condition Test Points. Each of the 5 throttle profiles were run at each test point.

Test Point	Altitude (ASL)	Mach Number
a*	0 ft	0
b	20,000 ft	0.6
c	30,000 ft	0.55
e	35,000 ft	0.8
d**	40,000 ft	0.8
f	5000 ft	0
g	5000 ft	0.2
h	10,000 ft	0
i	10,000 ft	0.2
j	15,000 ft	0.3

* Sea-level-static (SLS)
** Top of envelope

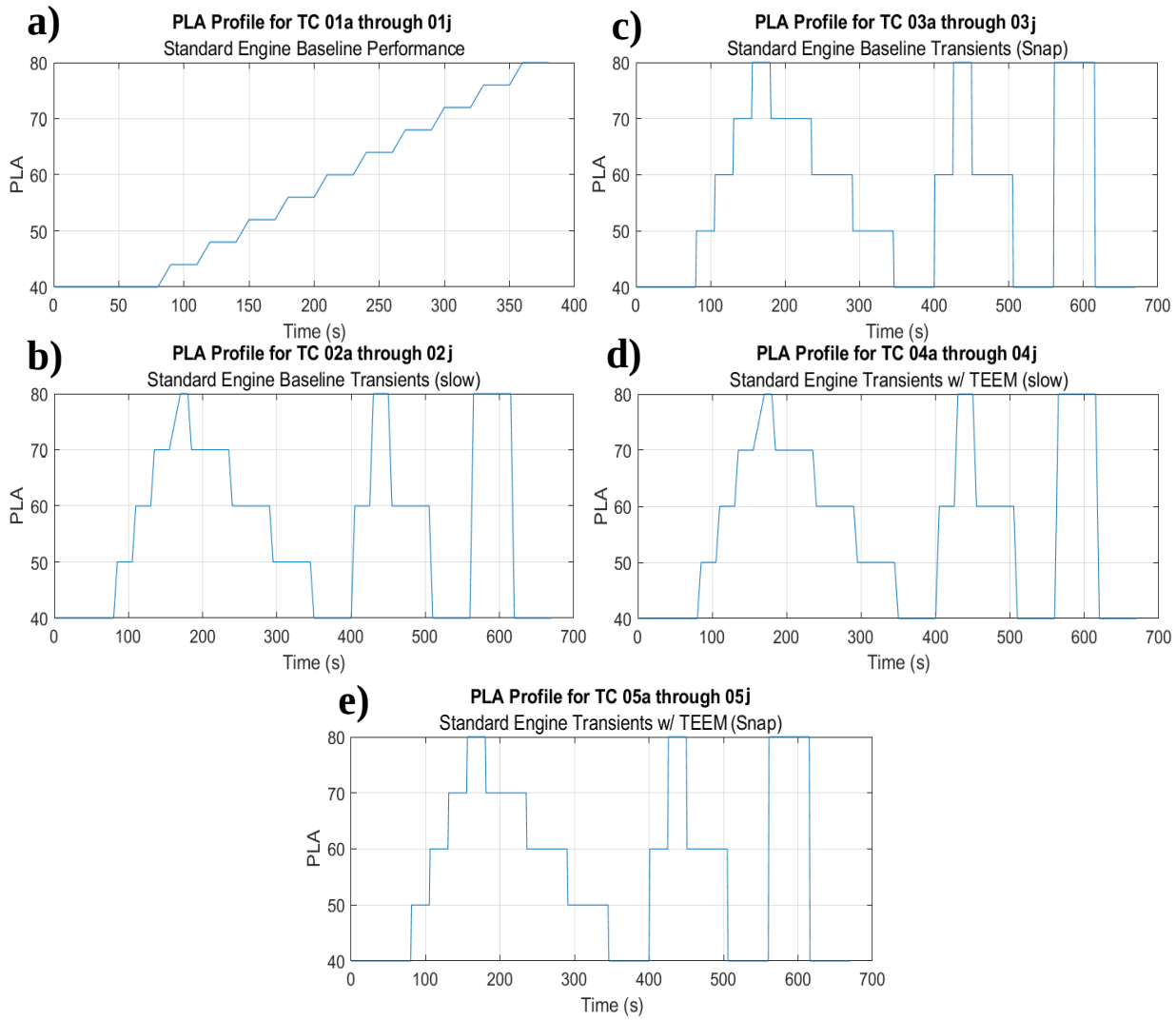

Figure A-1. Throttle profiles for test points (a) through (j):
(a) Throttle profile for Test Suite 01 – Steady state exploration of flight envelope with baseline controller.
(b) Throttle profile for Test Suite 02 – Slow throttle transients with baseline controller.
(c) Throttle profile for Test Suite 03 – Snap throttle transients with baseline controller.
(d) Throttle profile for Test Suite 04 – Slow throttle transients with TEEM controller.
(e) Throttle profile for Test Suite 05 – Snap throttle transients with TEEM controller.

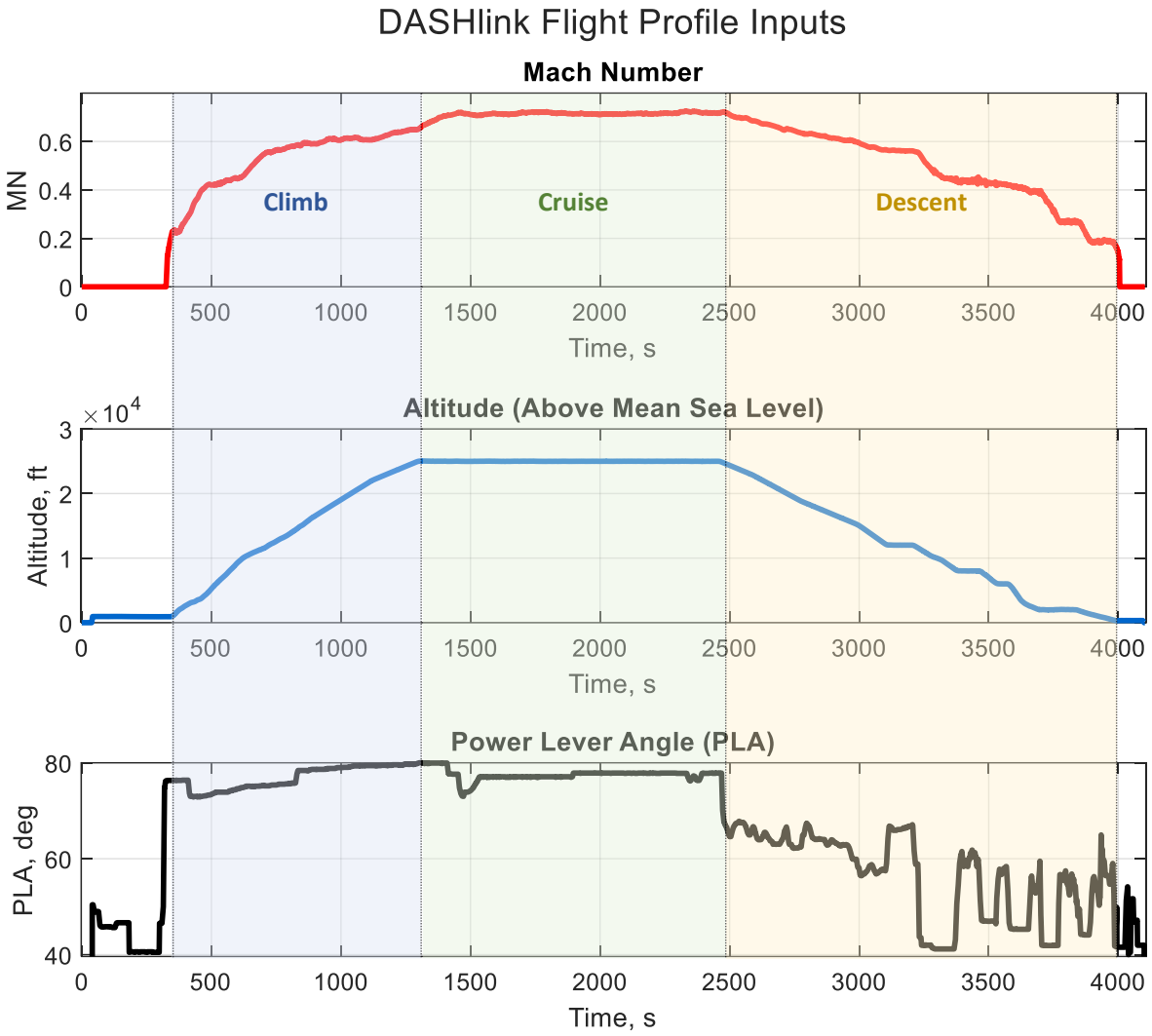

Figure A-2. Throttle, Altitude, and MN profiles for Test Card 6 – a simulated flight profile including taxi, takeoff and climb (in blue), cruise (in green), descent and landing (in yellow), and post-flight taxi. Data comes from the NASA's DASHlink website *[34]*

Acknowledgments

The authors acknowledge the Hybrid Thermally Efficient Core (HyTEC) project of the Advanced Air Vehicles Program (AAVP) for funding this research, as well as Joseph M. Haglage, Ying C. Cha, José G. Mendez, and the rest of the NEAT facility team at ATF for their support during the testing campaign.

References

[1] National Aeronautics and Space Administration, "NASA Aeronautics Strategic Implementation Plan," NASA Aeronautics Research Mission Directorate, Washington D.C., 2019.

[2] United States Federal Aviation Administration, "United States 2021 Aviation Climate Action Plan," FAA, 2021.

[3] National Aeronautics and Space Administration, "Sustainable Flight National Partnership," 2022. [Online]. Available: https://www.nasa.gov/sfnp/. [Accessed 3 2023].

[4] A. Schwab, A. Thomas, B. Jesse, E. Robertson and C. Scott, "Electrification of Aircraft: Challenges, Barriers, and Potential Impacts," National Renewable Energy Laboraty, Golden, CO, 2021.

[5] E. Piñero, "Electric vertical takeoff and landing aircraft dominate powered-lift community focus," Aerospace America, December 2022. [Online]. Available: https://aerospaceamerica.aiaa.org/year-in-review/electric-vertical-takeoff-and-landing-aircraft-dominate-powered-lift-community-focus/. [Accessed 9 March 2023].

[6] P. Marks, "eVTOL: Making the Electric Dream a Safe One," *Aerospace America*, September 2021.

[7] National, Academies of Sciences, Engineering, and Medicine, et al., "Commercial Aircraft Propulsion and Energy Systems Research : Reducing Global Carbon Emissions," National Academies Press, 2016, Washington, DC, 2016.

[8] R. H. Jansen, C. Bowman, A. Jankovsky, R. Dyson and J. Felder, "Overview of NASA Electrified Aircraft Propulsion Research For Large Subsonic Transports," in *AIAA Propulsion and Energy Forum*, Atlanta, GA, 2017.

[9] R. W. Dyson, "NASA Electric Aircraft Test bed (NEAT) Development Plan - Design, Fabrication, Installation," NASA/TM—2016-219085, Cleveland, OH, 2016.

[10] J. M. Haglage and T. W. Brown, "NASA Electric Aircraft Testbed (NEAT) Reconfiguration to Enable Altitude Testing of Megawatt-Scale Electric Machines," in *AIAA Propulsion and Energy Forum*, New Orleans, LA, 2020.

[11] National Aeronautics and Space Administration, "NASA Issues Award for Greener, More Fuel-Efficient Airliner of Future," NASA, 18 Jan 2023. [Online]. Available: https://www.nasa.gov/press-release/nasa-issues-award-for-greener-more-fuel-efficient-airliner-of-future. [Accessed 08 Mar 2023].

[12] D. L. Simon, J. W. Connolly and D. E. Culley, "Control Technology Needs for Electrified Aircraft Propulsion Systems," in *ASME Turbomachinery Technical Conference & Exposition*, Phoenix, AZ, 2019.

[13] J. W. Chapman, "Considering Turbofan Operability in Hybrid Electric Aircraft Propulsion System Design," in *AIAA SciTech Forum and Exposition*, National Harbor, MD, 2023.

[14] J. C. Gladin, C. Perullo, J. C. Tai and D. N. Mavris, "A Parametric Study of Gas Turbine Propulsion as a Function of Aircraft Size Class and Technology Level," in *AIAA SciTech Forum*, Grapevine, Texas, 2017.

[15] J. Kratz, D. Culley and G. Thomas, "A Control Strategy for Turbine Electrified Energy Management," in *AIAA Propulsion and Energy Forum*, Indianapolis, IN, 2019.

[16] J. Kratz, D. Culley and G. Thomas, "Turbine Electrified Energy Management (TEEM) For Enabling More Efficient Engine Designs," in *Joint Propulsion Conference*, Cincinnati, OH, 2018.

[17] J. Kratz, J. Connolly, A. Amthor, H. E. Buescher, S. J. Bianco and D. E. Culley, "Turbine Electrified Energy Management for Single Aisle Aircraft," in *IEEE/AIAA Electric Aircraft Technologies Symposium*, Anaheim, CA, 2022.

[18] R. H. Jansen, C. C. Kiris, T. Chau, G. K. W. Kenway, L. G. Machado and J. C. Duensing, "Subsonic Single Aft Engine (SUSAN) Transport Aircraft Concept and Trade Space Exploration," in *AIAA SciTech Forum*, San Diego, CA, 2022.

[19] C. L. Bowman, J. L. Felder and T. V. Marien, "Turbo- and Hybrid-Electrified Aircraft Propulsion Concepts for Commercial Transport," in *AIAA/IEEE Electric Aircraft Technologies Symposium*, Cincinnati, OH, 2018.

[20] Y. Cai, P. L. Chrysoula, J. Xie, J. K. Thind, M. M. Monjon, J. C. Gladin and D. N. Mavris, "System-level Trade Study of Hybrid Parallel Propulsion Architectures on Future Regional and Thin Haul Turboprop Aircraft," in *AIAA SciTech Forum*, National Harbor, MD, January 2023.

[21] J. D. M. Link C. Jaw, Aircraft Engine Controls: Design, System Analysis, and Health Monitoring, Reston, VA: AIAA Education Series, 2009.

[22] Z. S. Spakovszky, "Instabilities Everywhere! Hard Problems In Aero-Engines," in *ASME Turbo Expo*, Virtual, Online, 2021.

[23] G. C. Oates, Aerothermodynamics of Gas Turbine and Rocket Propulsion, Reston, VA: American Institute of Aeronautics and Astronautics, Inc., 1997.

[24] J. Kratz, D. Culley and G. L. Thomas, "Evaluation of Electrical System Requirements for Implementing Turbine Electrified Energy Management," in *AIAA Propulsion and Energy Forum*, Indianapolis, IN, 2019.

[25] J. Kratz, D. Culley and J. Lehan, "Transient Optimization for the Betterment of Turbine Electrified Energy Management (Submitted for Publication)," in *AIAA SciTech Forum and Exposition*, National Harbor, MD, 2023.

[26] J. Kratz and D. Culley, "Exploration of the Versatile Electrically Augmented Turbine Engine Gearbox Concept," in *AIAA Propulsion and Energy Forum*, Virtual, 2021.

[27] J. Chapman and J. Litt, "Control Design for an Advanced Geared Turbofan," in *AIAA/ASME/SAE/ASEE Joint Propulsion Conference*, Atlanta, GA, 2017.

[28] S. M. Jones, W. J. Haller and M. T. Tong, "An N+3 Technology Level Reference Propulsion System," NASA/TM-2017-219501, Cleveland, OH, 2017.

[29] J. Chapman, T. Lavelle, R. May, J. Litt and T.-H. Guo, "Toolbox for the Modeling and Analysis of Thermodynamic Systems (T-MATS) User's Guide," NASA/TM-2014-216638, January 2014.

[30] M. E. Bell and J. S. Litt, "Electrical Modeling and Thermal Analysis Toolbox (EMTAT) User's Guide," NASA/TM 20205008125, October 2020.

[31] S. J. Bianco and D. L. Simon, "Control and Scaling Approach for the Emulation of Sub-scale Dynamic Mechanical Loads," in *AIAA AVIATION/EATS*, San Diego, 2023.

[32] S. J. Bianco and D. L. Simon, "Sliding mode transient scaling controller for gas turbine engine emulation on an electric machine," in *AIAA Propulsion and Energy Forum*, Virtual Event, 2020.

[33] S. J. Bianco and et. al., "Hybrid-Electric Aero-Propulsion Controls Testbed Results with Energy Storage," in *AIAA EATS/AVIATION*, San Diego, 2023.

[34] B. Matthews, "DASHlink Sample Flight Data," NASA DASHlink, 29 November 2012. [Online]. Available: https://c3.ndc.nasa.gov/dashlink/projects/85/. [Accessed 2022].

[35] J. D. Mattingly, Elements of Gas Turbine Propulsion, New York: McGraw-Hill Inc., 1996.